

MODELLING AND SIMULATION OF A VIBROFORMER FOR CARBON ANODES USED IN ALUMINIUM PRODUCTION

Carbon anodes for aluminium smelting furnaces are formed by a vibration-compaction process. One seeks to control the operation of the vibroformer so as to optimise the properties of the anodes. A non-linear model of the vibroformer dynamics is formulated, solutions are computed and compared with data, and inferences about the compaction process are drawn.

1. Introduction

Aluminium is produced electrolytically from alumina dissolved in a molten salt (cryolite) bath. The anode in this process is a block of carbon. Approximately 0.4 - 0.45 kg carbon is consumed to produce 1 kg aluminium.

Anodes are produced from petroleum coke, recycled spent anodes (butts) and a binder pitch. A process flow chart is shown in figure 1. The coke and butt material are crushed to the desired size fractions. These are mixed and heated to 165°C. Pitch is added and the material is mixed further to form a paste. The paste is then formed into blocks weighing 1 - 1.2 tonnes in a vibratory compactor at 150°C (figure 2). The anodes are baked at 1100°C before use in the reduction cells.

The quality of the carbon anodes has a significant impact on the efficiency of the reduction process. One of the major steps which can affect quality is the vibratory forming. Poor anode compaction can result in

- low anode density
- high permeability which increases the reactivity of the carbon to air and CO_2 in the reduction cell
- cracks in the anode which increase the resistivity
- major cracks in the anode, leading to anode failure and replacement. This is extremely undesirable because it destabilises the cell, increases carbon consumption and results in high labour costs.

Defects observed prior to using the anodes lead to an anode rejection rate of around 2%. To reduce this rate, it is important to optimise compaction for all carbon plant operating conditions.

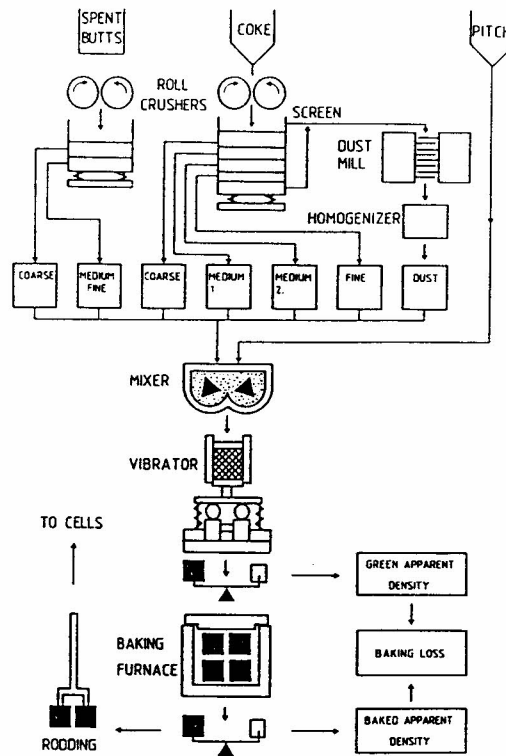


Figure 1: Carbon plant flowchart.

We note that vibration-compaction is more effective than monotone compression. First it allows transverse expansion to recover between impacts, so that jamming is avoided. Second it enhances mobility of solids and hence their reorganisation into a strong, compact matrix (in the manner of vibratory concrete compaction).

Monitoring of the vibroformer shows that the system is not linear (figure 3). The Study Group looked at the problem of developing and analysing a non-linear model. We also considered how to validate and how to utilise such a model.

The modelling focussed on the properties of the paste material. This is complex material which seemed not to be well understood. Initially it has characteristics similar to dry bitumen. The paste changes progressively during compaction: air is removed or compressed, stiffness increases and solid particles are spatially reorganised and redistributed. There was relatively little data available on the paste's rheological properties. We were not able therefore to directly formulate a model, carry out analysis and make predictions. Instead we tried to focus upon those properties which seemed important from an engineering point of view. This led us to consider possible mechanisms for

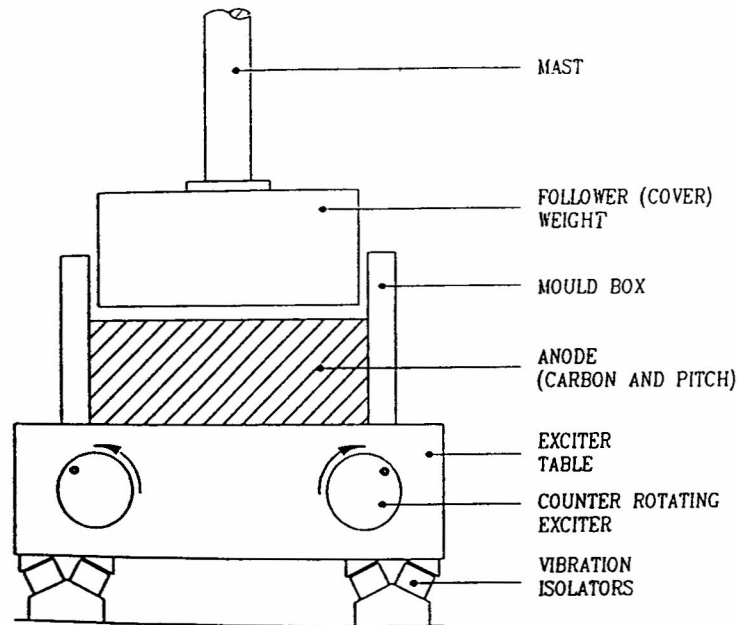


Figure 2: Schematical drawing of vibroformer.

the creation of the defects in anodes (Section 2); then to consider possible remedies for these defects and a consideration of how the non-linear model would assist the remedial process (Section 3). Having established clearer ideas about the potential uses of such a model, we were able to better consider a *purpose-built model*: one which was adequate for the purpose, but not too complex and unwieldy (Section 4). We performed some simulations of the model and compared them with data (Section 5). Section 6 contains some analysis and estimates, and conclusions are drawn in Section 7.

2. Possible causes of defects in anodes

In the absence of hard evidence on the causes of defects, we considered various hypotheses. Low anode density and high permeability appeared to be both manifestations of porosity or cavities in the anode. For porosity we have two basic hypotheses.

PH₁: Porosity results from inadequate compaction of the paste: possibly due to too stiff a paste, at too low a temperature: possibly due to an accidentally unfavourable vibration experience (Section 6 illustrates the variability and sensitivity of the vibroformer dynamics).

PH₂: Porosity results from excess pitch content in the paste. Loss of volatile fractions during baking then creates pores.

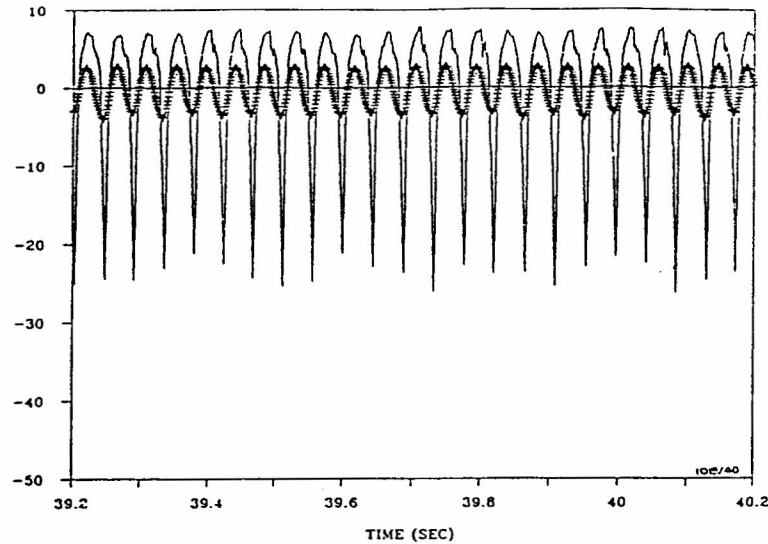


Figure 3: Measured downward acceleration of follower (solid line, m/sec^2) and relative displacement of anode and follower (hatched line, mm) at 22.5 cps. This trace is believed to be favourable to efficient compaction. (From Thrift, 1990.)

For cracks we also have two basic hypotheses.

*CH*₁: Cracks are caused by excessive impacts during compaction. The confinement of the material and its ductility suggest that this is not a brittle fracture process. Possibly, fracture is caused by longitudinal waves travelling vertically through the paste and creating tensile fractures. These should be horizontal, a prediction which could be tested by sampling.

*CH*₂: Cracks are caused by non-uniform density of green anodes, leading to non-uniform thermal expansion coefficients, leading in turn to thermal stress fractures during baking (Saeed, 1990, mentions this hypothesis).

Non-uniform density has implications for both porosity and cracking. Density of green anodes is found to be higher near the anode surface (Saeed, 1990). Two hypotheses were advanced for this non-uniformity.

*DH*₁: Non-uniform density is due to the migration of pitch and fine particles to regions of low-stress (the surfaces) during compaction. This effect should be more pronounced when pitch content and temperature are higher. Small increases in pitch content and temperature may be significant. The effect has been measured elsewhere in a continuous anode forming process and a theoretical analysis has been carried out (Bergstrom *et al.*, 1989). Since pitch has higher density than the solids, the hypothesis is consistent

with the data of Saeed (1990).

DH_2 : (Saeed, 1990) Higher density near the green anode surface results from more efficient compaction of the surface, due to inertia of the paste and friction between paste and mould-box.

It should be possible to distinguish between DH_1 and DH_2 by measuring density and spatial variation in green anode composition.

Combining these various hypotheses leads to predictions which could be tested. For example:

$PH_1 + DH_2$ imply that porosity is greater in the anode interior.

$PH_2 + DH_1$ imply that porosity is greater near the anode surface.

$CH_2 + DH_1$ imply that cracking is more severe in overpitched anodes.

3. Remedies for anode defects and the uses of a dynamical model

The remedy for a particular defect depends on which of the preceding hypotheses are ultimately borne out. At this stage we can only suggest remedies conditional on particular hypotheses. In each case we indicate how a dynamical model could be employed.

For example, under PH_1 the remedy would be to increase the vigour and/or duration of the compaction. But under $PH_1 + CH_1$, one should optimise this vigour and duration.

Under PH_2 , where the compaction process has little influence, the remedy is to improve the composition of the paste by better control of the mixing process prior to compaction. With the present set up at Comalco, this is not a practical solution. The options then are to accept or reject the anode in question. However, it is not easy to diagnose the condition of an anode by inspection. Since the vibration traces (see figure 3) are characteristic of anode properties, the traces might be used to diagnose defects. Here one needs a dynamical model to validate this process.

Under CH_1 , the simulations (Section 5) indicate that vibration frequency can be tuned so as to reduce the severity of impacts. One needs a dynamical model for this purpose.

Under CH_2 , the remedy of controlling paste composition is not practical, as mentioned before. Instead, one should be able to reduce the migration process by reducing the compaction time. First, one would need to use the initial vibration trace (perhaps 20 or 30 seconds) to diagnose the paste condition. Again, a dynamical model is needed.

4. Dynamical models

Having identified various diagnostic and control applications of a dynamical model, we now define a model. Figure 4 gives a schematic representation of the relevant masses, stiffnesses, dampings and forces. Here x_1 and x_2 are displacements relative to the undeformed spring positions. The rotating eccentric masses are replaced by a vertical, oscillatory force

$$c\omega^2 \sin \omega t \quad (1)$$

in which $c = 2mR$, m being the mass of each eccentric, R is the eccentric radius and ω the angular speed. Equation (1) gives the centripetal force exerted on the eccentrics by the base of the mould-box, if the mould box were stationary. The assumption or approximation here is that the control of the eccentrics is such that they do not react significantly to the mould-box motion. There is no horizontal force component because the contra-rotating eccentrics cancel this component. We followed Clark (1989) and took $c = 200,000/25^2 = 320N$ and ω in the vicinity of $25 \times 2\pi$ cps. The masses in figure 4 are

$$m_1 = 3650 \text{ kg}, \quad m_2 = 6270 \text{ kg}.$$

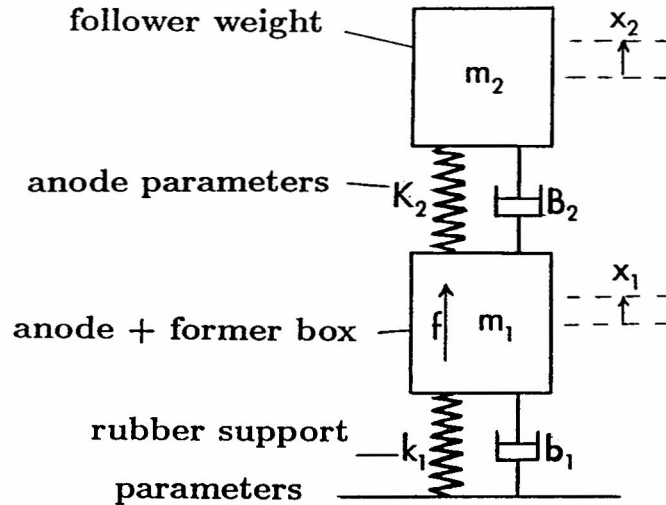


Figure 4: Representation of the mathematical model.

The rubber supports under the mould-box are represented by a linear spring and a linear damping force with constants

$$k_1 = 18.2 \text{ Nm}^{-1}, \quad b_1 = 5000 \text{ Nsm}^{-1}$$

respectively. The value of k_1 was supplied by the manufacturer, but the value b_1 was conjectured by Clark (1989).

The paste response was modelled by force terms

$$K_2 \times (x_2 - x_1) \quad (2)$$

$$B_2 \times (\dot{x}_2 - \dot{x}_1) \quad (3)$$

where K_2 and B_2 were taken to be functions of $x_2 - x_1$, viz.

$$K_2 = \begin{cases} k_2 & \text{if } x_2 \leq x_1 \\ 0 & \text{if } x_2 > x_1 \end{cases} \quad (4)$$

$$B_2 = \begin{cases} b_2 & \text{if } x_2 \leq x_1 \\ b_2^0 & \text{if } x_2 > x_1 \end{cases} \quad (5)$$

Equation (4) implies linear elastic response under compression but no force under extension. Thus the follower weight is assumed not to bond at all to the anode surface. The acceleration traces (*e.g.* figure 3) show this is usually true, as evidenced by the free fall acceleration ($-g$) of the follower weight. For overpitched, and hence sticky, paste, there is evidently some intermittent (random) bonding as shown in figure 10.

Equation (5) states that the paste applies linear damping to the follower weight when the two are in contact. When contact is broken ($x_2 > x_1$), the follower weight experiences smaller linear damping due to the friction arising from the snug contact between follower weight, mould-box, and paste between the two. We followed Clark (1989) and took

$$k_2 = 32.2 \times 10^6 \text{ Nm}^{-1}, \quad b_2 = 2000 \text{ Nsm}^{-1}$$

Values of b_2^0 in the range 100–500Ns/m were tried. We worried that $b_1 > b_2$, but had no evidence to the contrary. This model of the paste is obviously vastly simplified at best, but seems to be broadly consistent with available data.

Incorporating the model assumptions in Newton's equations of motion yields the non-linear equations

$$\begin{aligned} m_1 \ddot{x}_1 + k_1 s_1 + K_2(x_1 - x_2) + b_1 \dot{x}_1 + B_2(\dot{x}_1 - \dot{x}_2) + m_1 g &= c\omega^2 \sin \omega t \\ m_2 \ddot{x}_2 + K_2(x_2 - x_1) + B_2(\dot{x}_2 - \dot{x}_1) + m_2 g &= 0 \end{aligned} \quad (6)$$

Some numerical solutions (simulations) of these equations are given in the next section. Linear versions (constant K_2 and B_2) of these equations were studied by Clark (1989).

We briefly considered some other model equations:

1. In the early stages of compaction when the paste is quite fluid, a simple, inelastic impact model was postulated.
2. Because the accelerations in figure 3 show very sharp peaks, there is a very short time scale in the model. This time scale is shorter than the time for a compression wave to traverse the anode, so a more realistic model should represent the anode as a distributed mass. A damped one-dimensional wave equation is one possibility. This would be especially appropriate if CH_1 proves to be correct. Soil consolidation theory may also be appropriate.
3. In the direction of greater simplification, one might ignore the support rubbers in figure 4, and replace them with a static force $(m_1 + m_2)g$ to support the masses. Then equations (6) simplify to

$$\begin{aligned} m_1\ddot{x}_1 + B_2(\dot{x}_1 - \dot{x}_2) + K_2(x_1 - x_2) + m_1g &= (m_1 + m_2)g + c\omega^2 \sin \omega t \\ m_2\ddot{x}_2 + B_2(\dot{x}_2 - \dot{x}_1) + K_2(x_2 - x_1) + m_2g &= 0 \end{aligned} \quad (7)$$

These separate into simple independent equations for $x_1 - x_2$ and the centre of mass $(m_1x_1 + m_2x_2)/(m_1 + m_2)$.

Further work is needed in order to decide which of these various equations is most suited to the engineering application.

5. Simulations

The differential equations (6) were solved numerically using the IMSL routine IVPRK, which employs a Runge-Kutta-Verner fifth-order and sixth-order method. The results were generated in 1 millisecond time-steps over the 45 second compaction process. The results were plotted using S+. Computations were done on a SUN SPARCSTATION via an X-WINDOW terminal. The S+ plots were displayed on the terminal and printed on a laser printer. Special attention was paid to numerical accuracy and to the avoidance of numerical artifacts that might arise in either the computations or the plotting, due to time steps being too large.

Figure 5 shows an acceleration simulation over 1 second at 25 cps, which should be compared with the VIPAC data in figure 3. Of special interest is the 4 cycle modulation of the amplitude which also appears in figure 3. No such modulation appears in the linear model. Figure 6 shows acceleration data where period-doubling is evident, *i.e.* the follower weight experiences only one oscillation to every two cycles of the eccentrics

and the mould-box. Period doubling is also observed in simulations (figure 7). At higher frequencies, the model exhibits further period multiplying and also chaotic behaviour. The dynamics are very rich and sensitive to changes in parameters, as is typical of non-linear differential equations.

Figure 8 shows 45 second data for a “normal” vibration sequence; one which tends to produce satisfactory anodes. Figure 9 shows a simulated 45 second acceleration trace at 25 cps for the same parameters as figure 5. After the transient behaviour the oscillations are fairly stable and small, implying moderate impacts between paste and follower-weight. The transient portions of figures 8 and 9 should not be compared because the model assumes constant paste parameters (for compact anodes). After the transients, the data like the simulation, show stable oscillations of moderate amplitude, but with a modulation not present in the simulations.

Figure 10 shows data for a slightly lower vibration frequency. The simulation in figure 11 shows similar, large, erratic acceleration peaks. The data also shows randomly occurring downward accelerations greater than g , due to the follower weight sticking to the paste and being pulled down. This effect is excluded in the model, but it could be built in if necessary.

Figure 12 shows data for a so called *galloping* vibration which is considered undesirable. The very slow amplitude modulation at around 1/3 cps is roughly imitated in the simulation of figure 13.

6. Inferences from the linear model

In the linear model of Clark (1989), K_2 and B_2 are replaced by the constant k_2 and b_2 respectively. When the system is driven at a fixed frequency, the steady motion has only this frequency. For non-linear models, however, frequencies other than the driving frequency can appear in the steady state, as the figures show; for example the 4 cycle (\approx 6cps) oscillation of figures 3 and 5. Faced with the difficulty of analysing the non-linear model, we look to the linear model for indications.

To find the natural frequencies of the linear model, we substitute

$$x_i = A_i \exp(zt) \quad i = 1, 2, \quad (8)$$

with constant A_1 and A_2 , in the linear differential equations. Equating the determinant of the coefficient matrix of the A_i 's to zero gives

$$M_1 m_2 z^4 + [m_1 b_2 + m_2 (b_1 + b_2)] z^3 + [m_1 k_2 + m_2 (k_1 + k_2) + b_1 b_2] z^2 + (k_2 b_1 + k_1 b_2) z + k_1 k_2 = 0 \quad (9)$$

Using the parameter values from Section 5 and solving (9) numerically gives

$$z = -0.951 \pm i132.2, \quad -0.167 \pm i38.3 \quad (10)$$

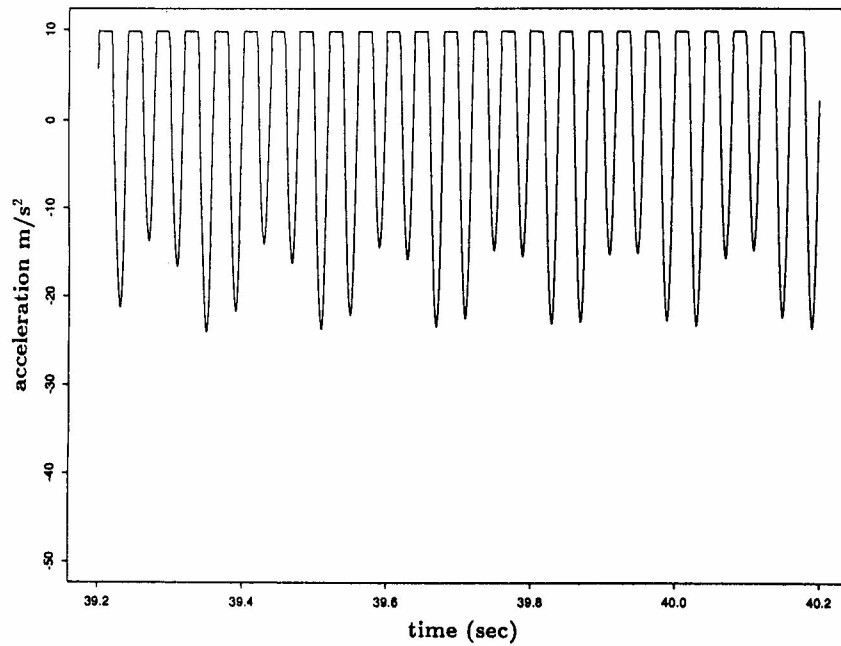


Figure 5: Simulated acceleration of the follower weight in the non-linear model with driving frequency 25 cps, $b_2^0 = 110$ Ns/m and the parameters of Section 4.

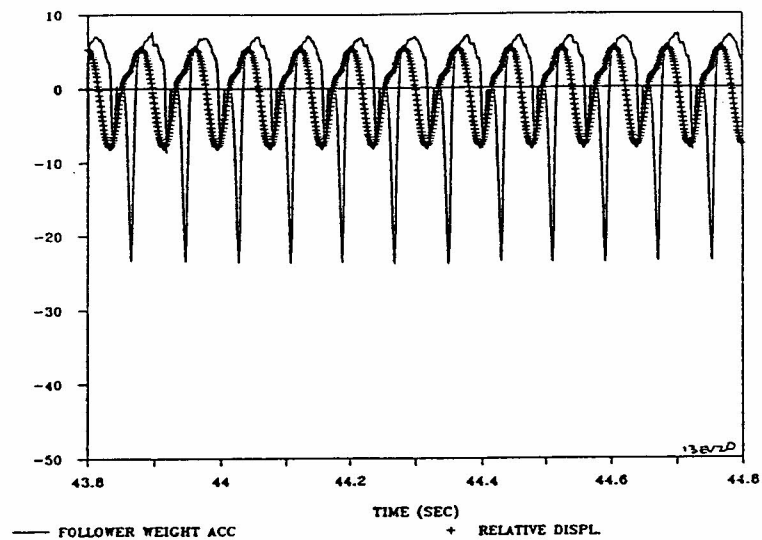


Figure 6: As in figure 3, but with driving frequency of 24.75 cps. (From Thrift, 1990.)

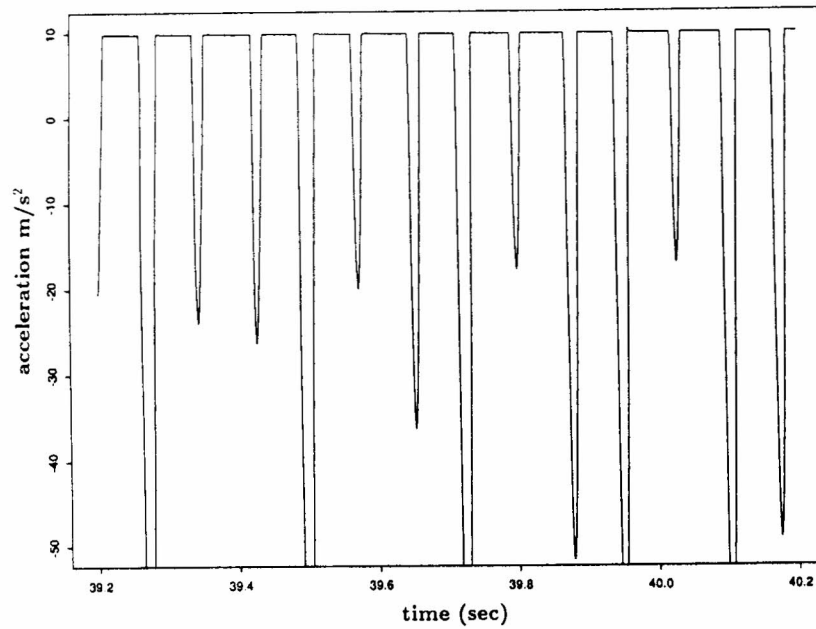


Figure 7: As in figure 5, but with driving frequency of 26.5 cps.

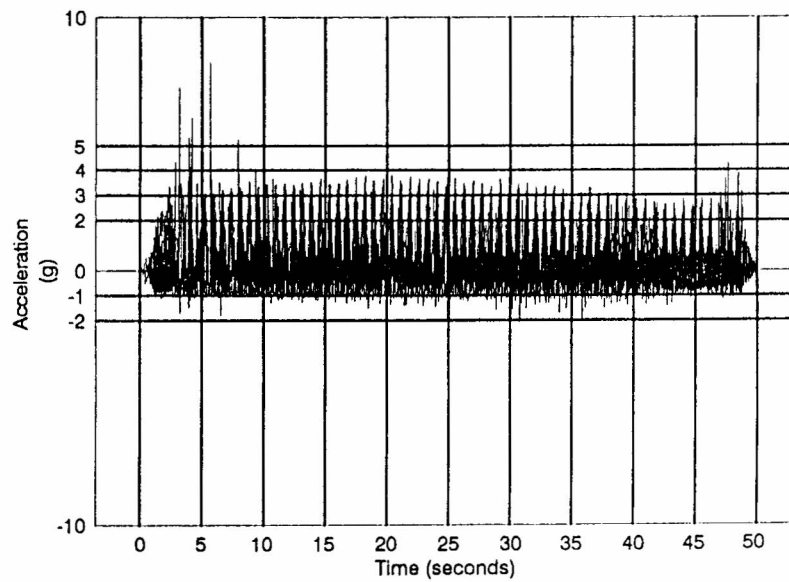


Figure 8: Measured (upward) acceleration envelope of the follower weight in a “normal” vibration over the full 50 sec. (From Sowerbutts, 1992.)

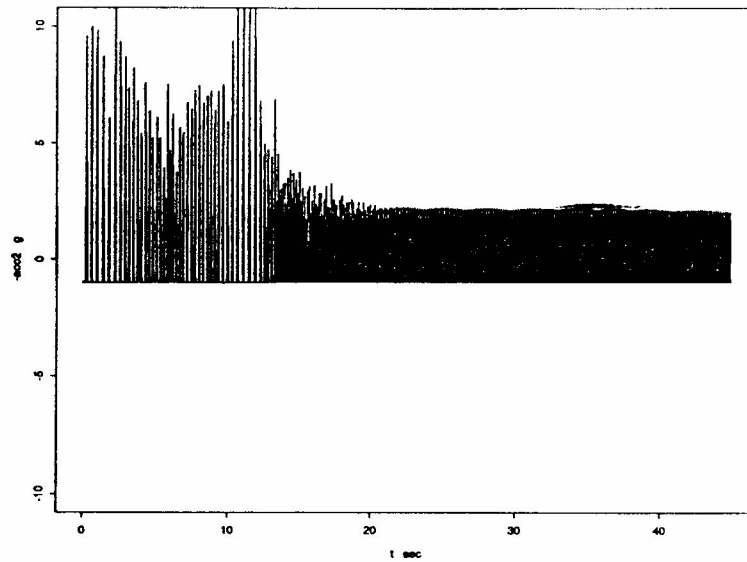


Figure 9: As in figure 5, but over 45 sec.

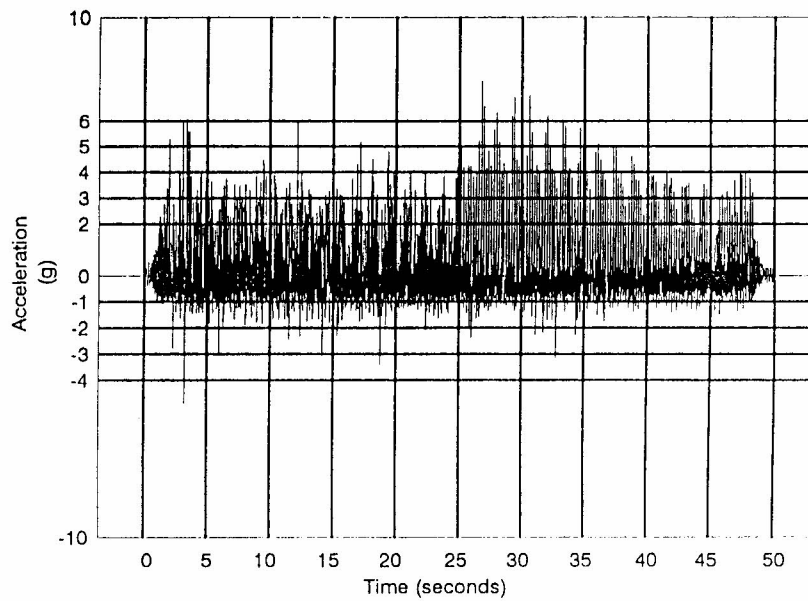


Figure 10: Measured acceleration envelope of the follower weight in a “quiet galloping” vibration. (From Sowerbutts, 1992.)

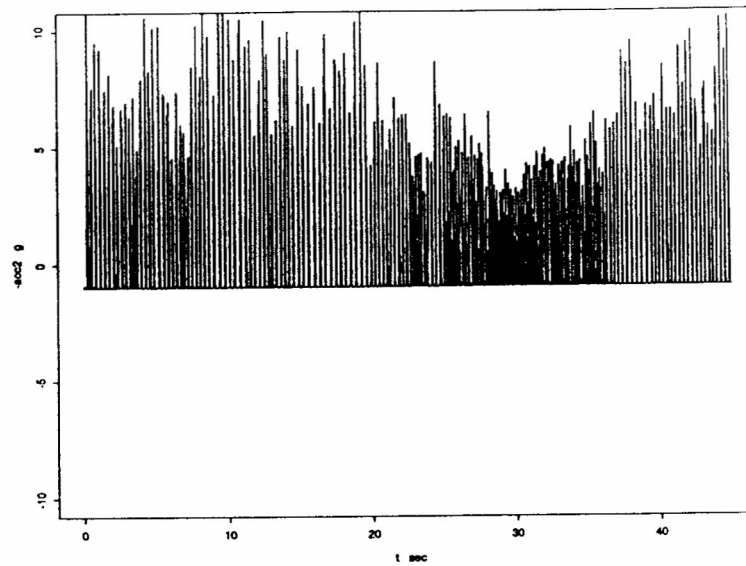


Figure 11: As in figure 9, but with $b_2^0 = 500$ Ns/m and driven at 26 cps.

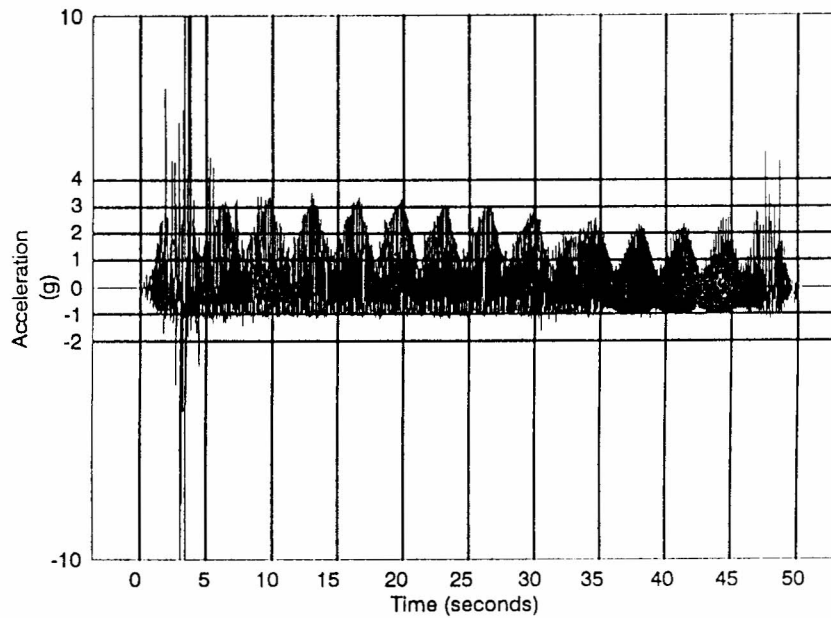


Figure 12: Measured acceleration envelope of the follower weight in a "galloping" vibration. (From Sowerbutts, 1992.)

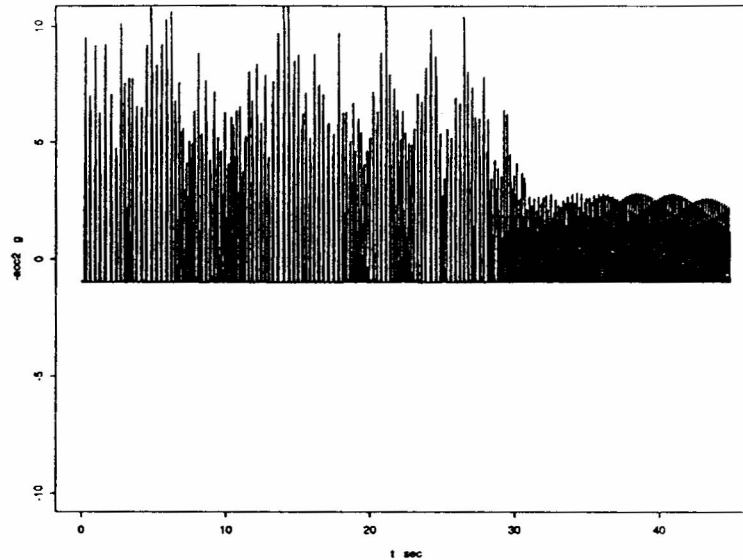


Figure 13: As in figure 11, but driven at 25 cps.

The negative real parts imply damping. The imaginary parts, on division by 2π , give the frequencies

$$21.04 \text{ and } 6.09 \text{ cps} \quad (11)$$

The normal mode corresponding to the lower frequency has the 2 masses oscillating approximately in phase *i.e.* $A_1 \approx A_2$ and $x_1 \approx x_2$. To check this, note that it would imply a frequency

$$[k_1/(m_1 + m_2)]^{1/2}/2\pi = 6.8 \text{ cps} \quad (12)$$

which approximates the lower natural frequency.

Possibly this lower frequency mode is the source of the 6 cps modulation observed in the simulations (figure 5) and the measured accelerations (figure 3). The 21 cps frequency may be less relevant to the non-linear model, because it corresponds to approximately opposed motion of m_1 and m_2 , and the interaction between the m 's is distinctly different in the non-linear model.

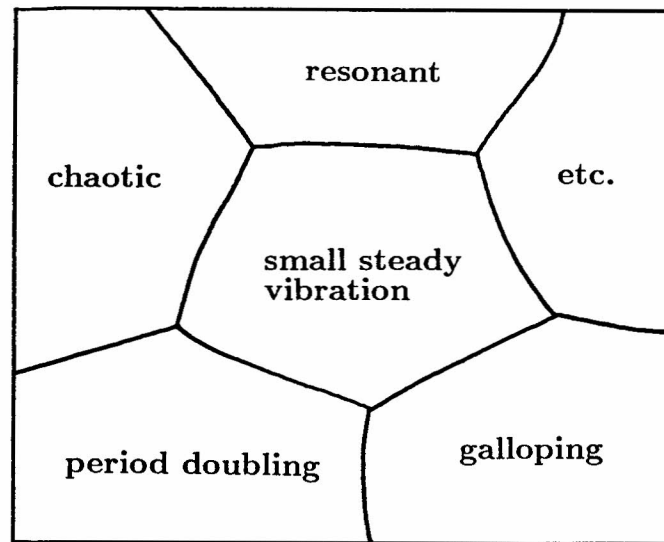


Figure 14: Hypothetical subdivision of the relevant parameter space according to dynamical behaviour.

7. Summary and future directions

1. A non-linear differential equation model (6) was shown to imitate many effects observed in the dynamics of the vibroformer.
2. A number of possible uses of the model were identified. The uses include diagnosis and control.
3. Suggestions were made for further studies and measurements which would help to test the various hypotheses advanced in Section 2 and help to validate the model.

Much more extensive simulations are needed in order to use the model in the way suggested. One needs to characterise the dynamics for any choice of parameters in the range of practical interest, in the manner of figure 14. Such characterizations exist for well known equations like the Duffing equation with a periodic forcing term (see Davis (1962, figures 33 and 36). In our case, a map like figure 14 could be constructed in a straightforward way by choosing a grid of points in the parameter space and doing a simulation for each point.

Acknowledgements

The moderator of this problem (David Gates) acknowledges the important contributions of the group which participated in the discussion. Special thanks go to Chris Gallagher of Comalco and to Basil Benjamin, Neville Fowkes and John Ockendon. John Sowerbutts of Comalco is thanked for helpful comments on the manuscript.

References

- H.T. Davis, *Introduction to non-linear differential and integral equations* (New York, Dover, 1962).
- T. Bergstrom, S. Cowley, A.C. Fowler & P.E. Seward, "Segregation of carbon paste in a smelting electrode", *IMA J. App. Math.* 43 (1989), 83-99.
- G.J. Clark, Untitled [Linear differential equation modelling of the vibroformer], Comalco Research Centre, Carbon group, *Notebook no. S48* (1989).
- C. Salisbury & G.Clark, "NZAS anode vibroformer modelling", Comalco Research Centre, *Technical Report CRC/TR/89/131* (1989).
- M. Thrift, "Investigation of anode former compaction dynamics to improve anode production. Stage 1 - initial measurements", *VIPAC Report No. 72354* (1990).
- I. Saeed, "Green core trial", Boyne Smelters, *Report LP 122402, IM/2* (1990).
- J. Sowerbutts, "NZAS vibroformer signal analysis results", Comalco Research Centre *Technical Report CRC/TR/92/2* (1992).